Shear-induced melting of smectic-*A* liquid crystals

N. J. Mottram,[1,*] T. J. Sluckin,[1,2] S. J. Elston,[1,3] and M. J. Towler[1,4]
[1]*Department of Mathematics, University of Strathclyde, 26 Richmond Street, Glasgow G1 1XH, United Kingdom*
[2]*Faculty of Mathematical Studies, University of Southampton, Highfield, Southampton SO17 1BJ, United Kingdom*
[3]*Department of Engineering Science, University of Oxford, Parks Road, Oxford OX1 3PJ, United Kingdom*
[4]*Sharp Laboratories of Europe Ltd., Edmund Halley Road, Oxford Science Park, Oxford OX4 4GA, United Kingdom*
(Received 22 February 1999; revised manuscript received 25 May 2000)

A numerical and analytical analysis of shear-induced melting in smectic-*A* liquid crystals is presented. Based on a Landau expansion of the complex smectic order parameter, equations governing the phase and amplitude of the local density modulation are found. Numerically solving these equations indicates that for a range of parameter values a first-order transition, from a shear-stressed to a more relaxed state, is periodically encountered as the total shear is increased. Suitable approximations allow the analytic determination of certain characteristics of this first-order transition.

PACS number(s): 61.30.Cz, 61.30.Gd

I. INTRODUCTION

The liquid crystalline smectic-*A* phase exhibits order intermediate between that of a solid and a liquid [1]. Its defining quality is the existence of one-dimensional positional ordering in the form of a periodic molecular density function forming a layered structure. In equilibrium, the unconstrained liquid crystal layers are uniformly separated by a distance $2\pi/q$, where q is the preferred wave number of the density fluctuations. However, out of equilibrium, or in the presence of boundary conditions that disturb the preferred equilibrium configuration, the layer structure can be significantly different. In this paper, we discuss, quantitatively, one situation in which this layer structure may be distorted.

We consider a smectic-*A* liquid crystal sample initially in the so-called bookshelf geometry, in which the nematic director is aligned in the same uniform $\hat{\mathbf{x}}$ direction on each surface of the cell, which lie in the *xy* plane (Fig. 1). The consequence of these *homogeneous* boundary conditions is that the smectic layers form a bookshelflike structure, in the *yz* plane. However, this bookshelf configuration may be disturbed by a sufficiently strong perturbation.

Such a perturbation may be induced simply by changing the sample temperature, thus changing the preferred thermodynamic layer spacing. The bookshelf structure deforms into a V-like layer configuration, known as the chevron structure [2]. The chevron structure has been much studied, because its behavior plays a crucial role in surface stabilized ferroelectric liquid crystal cells that are of great commercial interest due to their considerable potential for exploitation in display devices.

Phenomenological theories of chevron structures typically assume that there exists a surface memory effect that anchors the layers at the cell surfaces while the natural layer spacing changes in the bulk of the cell. The mismatch between the layer thickness at the surface and within the cell is believed to induce the chevron structure. However, the precise microscopic physics behind chevron formation remains poorly understood.

In an effort to explain the surface interaction, Cagnon and Durand [3] performed an experiment in which they sheared a cell filled with a smectic-*A* liquid crystal, moving one wall laterally with respect to the other. Accurately measuring the very small transmitted stress, they found periodic discontinuities superimposed on a monotonic, background stress. They interpreted these discontinuities as slipping of the layers with respect to the walls. These results were explained as the bookshelf geometry first tilting as it follows the motion of the walls, and then slipping as the original bookshelf geometry, with lower free energy, reforms. In this way Cagnon and Durand were able to estimate the energy associated with the surface-memory-induced layer anchoring at the walls.

This paper aims to examine the general question of the interplay between the energetically favorable bookshelf geometry and an applied shear stress that distorts it. Elston and

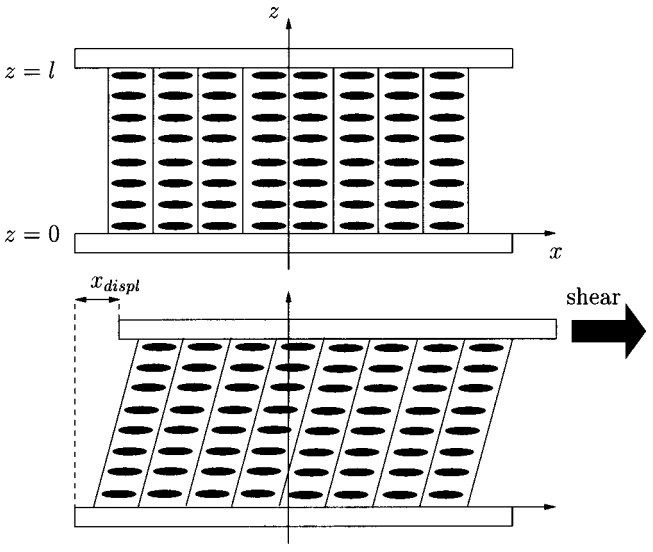

FIG. 1. Cell configuration: Smectic-*A* material is sandwiched between glass plates at $z=l$ and $z=0$ where the director is aligned homogeneously. The shear force applied to the upper glass plate induces layer distortion.

*Author to whom correspondence should be addressed.

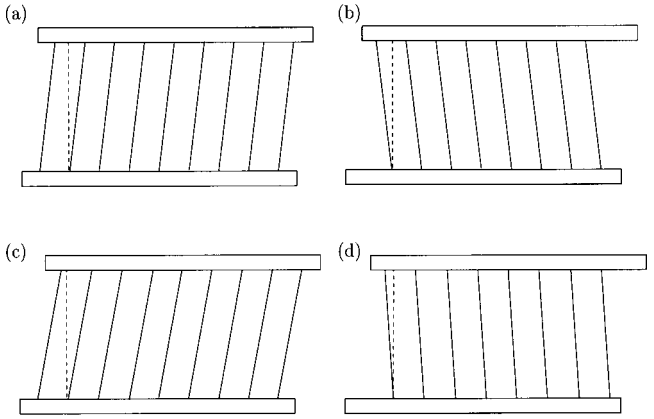

FIG. 2. (a), (b) Energetically equivalent tilted layers for $\tau = \pi \,(\mathrm{mod}\, 2\pi)$. As the shear is increased past π, the two stable configurations are a metastable, supersheared state (c) and a reverse tilt state (d). A first-order transition between these *topologically* distinct states involves breaking up or melting the layer structure.

Towler [4] have previously shown, using an idealized model, that the presence of a large interwall shear can lead to a significant reduction in the smectic order parameter in the middle of the cell, and sufficiently large shear can, under some circumstances, destabilize the deformed bookshelf geometry. In this paper, we aim to extend this work to give a coherent picture of the whole phenomenon. In so doing, we find a complex structure of stable, metastable, and unstable states and describe the associated transitions between them.

In Sec. II we will give a physical overview of the complete problem, and provide the reader with a summary of our results. In Sec. III we present the model in detail and introduce the principal approximations subsequently used. A numerical study of the solutions of the governing equations is given in Sec. IV, the important aspects of which we consider in more detail using a number of analytical techniques in Sec. V. Finally, in Sec. VI, we summarize and discuss possible future extensions of these results.

II. PHYSICAL UNDERSTANDING

In this section we give a brief overview of the physics involved in the model we consider. The most important assumption we will make in this paper is to suppose that the layer anchoring is infinite. Thus, when the initial bookshelf geometry is perturbed the layers are forced, at least initially, to follow the moving surfaces (Fig. 1). We remark that the assumption of infinite rather than finite anchoring is not essential, although some of the most striking results in this paper depend on having relatively strong surface smectic anchoring.

The smectic order parameter is a two-component object [5], usually denoted by a complex number

$$\Psi = \rho e^{i\Phi}, \tag{1}$$

where ρ is the degree of order, usually thought of as being equivalent to the amplitude of the smectic density wave, and Φ is its phase. The nature of the order parameter suggests that there is considerable similarity between the statistical mechanics of smectics and $n=2$ spin systems described by the classical XY model [6–8]. Indeed, it was the analogy between superconductors and smectic liquid crystals that first led de Gennes to use this order parameter. However, unlike in classical XY models, the low temperature phase is not constant, but a layered phase with wave number q in the direction parallel to that of the nematic director $\hat{\mathbf{n}}$.

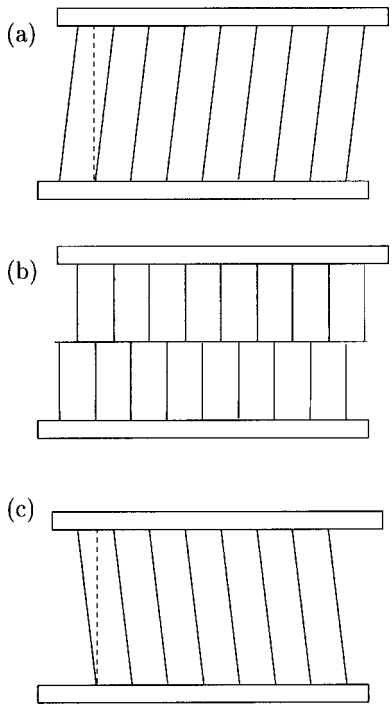

FIG. 3. For thin cells, as shear increases, (a) the layers start to melt at the center so that, at complete mismatch, the phase difference of $+\pi$ and $-\pi$ are indistinguishable, (b) At larger shear, (c), the layers reform with reverse tilt.

In considering this system, it will be useful to measure the degree of stress by the amount of relative lateral displacement x_{displ} of the walls (Fig. 1). This may be more conveniently marked by the degree of layer mismatch $X_{\mathrm{displ}} = x_{\mathrm{displ}}/d_{\mathrm{layer}}$, the relative lateral displacement of one wall with respect to the other in units of the smectic layer thickness d_{layer}. The quantity $\tau = 2\pi X_{\mathrm{displ}}$ is the equivalent quantity in radians; it is the change in phase between points that would lie opposite to each other in the bookshelf geometry.

The natural length scale in this system is the smectic correlation length ξ. This is the length scale on which changes in the bulk smectic order may be expected to occur. We will find different behavior depending on whether the ratio of the cell thickness to this correlation length l/ξ is much greater than or much less than unity, with a sharp crossover between the two regimes. For us, thin films are those for which $l/\xi \leqslant 1$.

It is useful to consider what we expect to happen when one cell surface is sheared with respect to the other. For extremely small shears $-\frac{1}{2} \leqslant X_{\mathrm{displ}} \leqslant \frac{1}{2}$, or equivalently $-\pi \leqslant \tau \leqslant \pi$, the layers will bend in order to connect between the surfaces. Consequently, there will be an increase in the curvature free energy. However, in order to minimize this curvature free energy the smectic liquid crystal may reduce its order parameter in the bulk of the system which, due to the symmetry of the system, will reach a minimum in the center of the cell.

Let us now consider what happens when the phase mis-

match is exactly π. The smectic layers at the cell surfaces will be *completely mismatched*, i.e., exactly out of phase. There are now two energetically equal layer configurations. The layer at one surface is positioned exactly between two layers at the opposite surface and may join to either one. The crucial question is whether these states are physically distinct.

If they are different (Fig. 2), then as the phase mismatch is increased through π the sheared state becomes a metastable state, and the previously stable free-energy branch is extended into a metastable region [Fig. 2(b)]. We shall refer to this state as supershear. The globally stable state is now that which involves an effective phase difference across the sample between $-\pi$ and 0 [Fig. 2(c)] i.e., layers with reverse tilt. The *topologically* distinct, metastable, supersheared state has a phase difference $|\tau|>\pi$. Reaching the stable state from the metastable state involves breaking up or melting the layer structure within the sample and reforming the layers in such a way that phase difference is reduced. Transfer between the two branches of the curve in this case necessarily involves a first-order phase transition.

By contrast, we can imagine that at complete mismatch the phase difference of $+\pi$ and $-\pi$ are indistinguishable (see Fig. 3). If this is the case, symmetry necessarily demands that the system melt in the center of the cell [Fig. 3(b)]. Only if the layers melt in the middle of the cell will it be possible for there to be a unique ground state with complete mismatch. In this case, the phase is undefined in the center of the cell, and if the phase is undefined, then the degree of order must be zero. At larger shear, reverse tilt layers reform with a phase difference across the sample between $-\pi$ and 0 [Fig. 3(c)].

We will subsequently discover that the second, melting, scenario occurs for thin cells, for then the energy associated with tilting a layer is relatively large. By melting at $|\tau|=\pi$ and then reforming for $|\tau|>\pi$, the large layer tilt is avoided. By contrast for thick cells, tilting is preferred. Eventually, for larger shears, the metastable state reaches a spinodal line and destabilizes. We shall find, unsurprisingly, that for sufficiently thick films, the critical shear is proportional to the thickness, and that in nondimensional units is of the order of unity.

Between these two régimes is a critical cell thickness of $l=l_c$ where the behavior at $\tau=\pi$ changes. At the critical thickness l_c equilibrium melting at complete mismatch no longer occurs. An important part of the analysis will consist of an examination of the stability of the equilibrium melted state at $\tau=\pi$. Such a state always occurs, but whereas it is a stable state for thin films, for thick films it is unstable. Analysis of the critical point will give rise to critical exponents associated with the onset of supershear.

For very thick films $l/\xi\gg 1$, there will be many metastable supersheared states for a given τ. The loss of stability of the highest energy supersheared state moves the system to the next state down in energy. Because the supersheared states are topologically distinct, the natural language with which to classify them is also topological. It will turn out that a solution of the governing equations for Ψ can be classified in terms of its trajectory in the complex plane. Such a trajectory possesses a winding number, or more technically a Morse Index, which counts the number of times the trajectory orbits the origin. The loss of stability of the supersheared state involves the mutual annihilation of stable and unstable states with the same Morse Index and consequently the trajectory decays to a new state with its Morse Index decreased by one.

In this section, we have seen how shearing a smectic-*A* liquid crystal in a bookshelf configuration can lead to a complex physical phenomena. In the next section, we shall develop a mathematical formalism to describe the physical ideas presented here.

III. MODEL AND BASIC THEORY

A. Landau-de Gennes Theory

We will use the energy expression used previously by Kralj and one of the present authors [9].

$$F=\int d\mathbf{r}\Big[A|\Psi|^2+\frac{B}{2}|\Psi|^4+\zeta_{\parallel}|(\hat{\mathbf{n}}\cdot\boldsymbol{\nabla}-iq)\Psi|^2+\zeta_{\perp}|(\hat{\mathbf{n}}\times\boldsymbol{\nabla})\Psi|^2+\tfrac{1}{2}K_{11}(\boldsymbol{\nabla}\cdot\hat{\mathbf{n}})^2+\tfrac{1}{2}K_{33}[\hat{\mathbf{n}}\times(\boldsymbol{\nabla}\times\hat{\mathbf{n}})]^2\Big]. \tag{2}$$

The reader should be aware that this form of the free energy is different from that used in de Gennes and Prost (p. 510) [1]. The difference occurs in the form of the gradient terms. In the present case, the gradient terms are formed using a mass tensor that is diagonal in a frame of reference fixed with respect to the cell (a laboratory frame of reference) while the de Gennes gradient terms are derived from a mass tensor that is diagonal with respect to a frame of reference defined by the director (an internal frame of reference).

For small deformations the two formulations are equivalent. For large deformations there will be differences, which will be the focus of further research. We note, however, one intuitive advantage of this formulation. When the layers are reduced in thickness, on purely geometric grounds we might expect a director tilt that compensates for this in just such a way that the wave number in a direction parallel to the director remains constant. In Eq. (2) the $\zeta_{\parallel}$ term favors a director tilt that compensates for layer reduction in thickness in just this way.

In undistorted equilibrium, the smectic order parameter is determined by the first two terms of the above energy. Minimization of these terms leads to the bulk smectic order parameter modulus, $\rho_c=(-A/B)^{1/2}$. Stability of the smectic phase requires, as in all theories of this type, that $A<0$ and $B>0$. In Eq. (2) the $\zeta_{\parallel}$ term is associated with changes in the smectic density wave and, as we shall indicate later in this section, in the present situation the cell surfaces induce a preferential bulk layer density wave number in the x direction of the value q. In Eq. (2), the $\zeta_{\perp}$ term is normally associated with departures of the director from the smectic layer normal. The last two terms represent the elastic energy of distortions to the nematiclike director $\hat{\mathbf{n}}$ within the smectic layer.

The system is infinite in the $\hat{\mathbf{x}}$ and $\hat{\mathbf{y}}$ directions, and placed in a cell with flat walls at $z=0$ and $z=l$ (Fig. 1). We choose boundary conditions that give a homogeneous alignment:

$$\hat{\mathbf{n}}(z=0)=\hat{\mathbf{n}}(z=l)=\hat{\mathbf{x}}, \tag{3a}$$

$$\Psi(z=0)=\rho_c e^{iqx}, \tag{3b}$$

$$\Psi(z=l)=\rho_c e^{i(qx+\tau)}. \tag{3c}$$

These boundary conditions fix the smectic order parameter such that the phase Φ is strongly anchored at the surface and the modulus ρ remains at the bulk equilibrium value. Such strong anchoring conditions exert great influence on the structure of the smectic layers and weaker conditions such as the introduction of a *surface energy*, will lead to a different form of stress relaxation within the bulk of the cell.

We shall suppose that, for zero shear, the system is homogeneous in the $\hat{\mathbf{x}}$ direction and changes in Ψ are wholly induced by the sheared layering at the boundary. We similarly suppose the system to be completely homogeneous in the $\hat{\mathbf{y}}$ direction. It will be useful to parameterize the order parameter as follows:

$$\Psi(x,z)=\rho(z)e^{i\Phi(x,z)}=\rho(z)e^{i[qx+\phi(z)]}=\psi(z)e^{iqx}, \tag{4}$$

where $\psi(z)=\rho(z)e^{i\phi(z)}$. This parameterization separates out the explicit x-dependent layer behavior, given by $\Phi_0(x)=qx$, from the shear-induced variation across the cell, given by $\phi(z)$. The Ψ boundary conditions [(3b),(3c)] can now be rewritten as

$$\psi(z=0)=\rho_c, \tag{5a}$$

$$\psi(z=L)=\rho_c e^{i\tau}. \tag{5b}$$

Thus the phase $\phi(z)$ ranges from 0 to τ across the cell, though of course layer slippage may allow the phase to vary between 0 and $\tau\pm 2n\pi$ where n is an integer.

The free energy may now be written as a functional of $\rho(z)$ and $\phi(z)$ rather than $\Psi(\mathbf{r})$. The nematiclike director, which lies in the xz plane, may be written as $\hat{\mathbf{n}}=(\cos\theta,0,-\sin\theta)$, so that $\hat{\mathbf{n}}$ is tilted with respect to the x direction by an angle θ. For simplicity, we use a one constant approximation for the nematic elastic constants: $K_{11}=K_{33}=K$. We then obtain the following result:

$$\begin{aligned}F=\int_0^l dz\Bigg[&a\rho^2+\frac{b}{2}\rho^4+\frac{K}{2}\left(\frac{d\theta}{dz}\right)^2+\zeta_{\parallel}\Bigg\{\left[\left(\frac{d\rho}{dz}\right)^2+\rho^2\left(\frac{d\phi}{dz}\right)^2\right]\\&\times\sin^2\theta+\rho^2q^2(1-\cos\theta)^2+2\rho^2q\frac{d\phi}{dz}\sin\theta(1-\cos\theta)\Bigg\}\\&+\zeta_{\perp}\Bigg\{\left[\left(\frac{d\rho}{dz}\right)^2+\rho^2\left(\frac{d\phi}{dz}\right)^2\right]\cos^2\theta\\&+\rho^2q^2\sin^2\theta+2\rho^2q\frac{d\phi}{dz}\sin\theta\cos\theta\Bigg\}\Bigg].\end{aligned} \tag{6}$$

In this paper, we will assume that changes to the layer density wave are energetically unfavorable compared to other forms of distortion within the liquid crystal. In other words we assume that $\zeta_{\parallel}$ is very large compared to all other energy coefficients. It can then be shown (see the Appendix) that, except for very small amounts of shear when the molecular tilt angle follows the layer tilt angle and remains parallel to the layer normal, we may assume that $\theta=0$. Therefore, although tilted layers tend to rotate the director in order that it remain normal to them for small tilt angles, this tendency is suppressed by the fact that the layers would then have the wrong thickness along the x direction. For larger layer tilt angles the compression energy term dominates and forces the director angle to be approximately zero ($\theta\approx 0$) throughout the sample. Although this approximation limits the validity of our analysis, we will later show that the important processes in this system occur at relatively large shear values, at which our equations are valid.

Substituting this result into Eq. (6) yields the following form of the free energy, which will subsequently be used in this paper:

$$F=\int_0^l dz\left[a\rho^2+\frac{b}{2}\rho^4+\zeta_{\perp}\left\{\left(\frac{d\rho}{dz}\right)^2+\rho^2\left(\frac{d\phi}{dz}\right)^2\right\}\right]. \tag{7}$$

B. Scaling

As previously discussed, the fundamental length scale in this problem is the relaxation length for smectic order fluctuations

$$\xi=\left(\frac{\zeta_{\perp}}{|a|}\right)^{1/2}, \tag{8}$$

which is the length scale on which changes in the bulk smectic order may be expected to occur. The free-energy functional (7) can be nondimensionalized using the following scalings:

$$\tilde{\psi}=\frac{\psi}{\rho_c}, \tag{9a}$$

$$r=\frac{\rho}{\rho_c}, \tag{9b}$$

$$\tilde{z}=\frac{z}{l}, \tag{9c}$$

$$d=\frac{l}{\xi}, \tag{9d}$$

$$\tilde{F}=\frac{b}{2ld^2}F. \tag{9e}$$

It is mathematically more convenient to scale distance with respect to system size, and absorb the thickness into the equations rather than the boundary conditions. Dropping the tildes from the resulting expressions yields the following renormalized functional:

$$F=\int_0^1 dz\left[\frac{1}{4}(r^2-1)^2+\frac{1}{2d^2}(r'^2+r^2\phi'^2)\right], \tag{10}$$

where we have added a constant term in order to simplify the form of the smectic potential and derivatives with respect to z are denoted by primes. To this functional we append the boundary conditions

$$r(0)=1,\quad \phi(0)=0, \tag{11a}$$

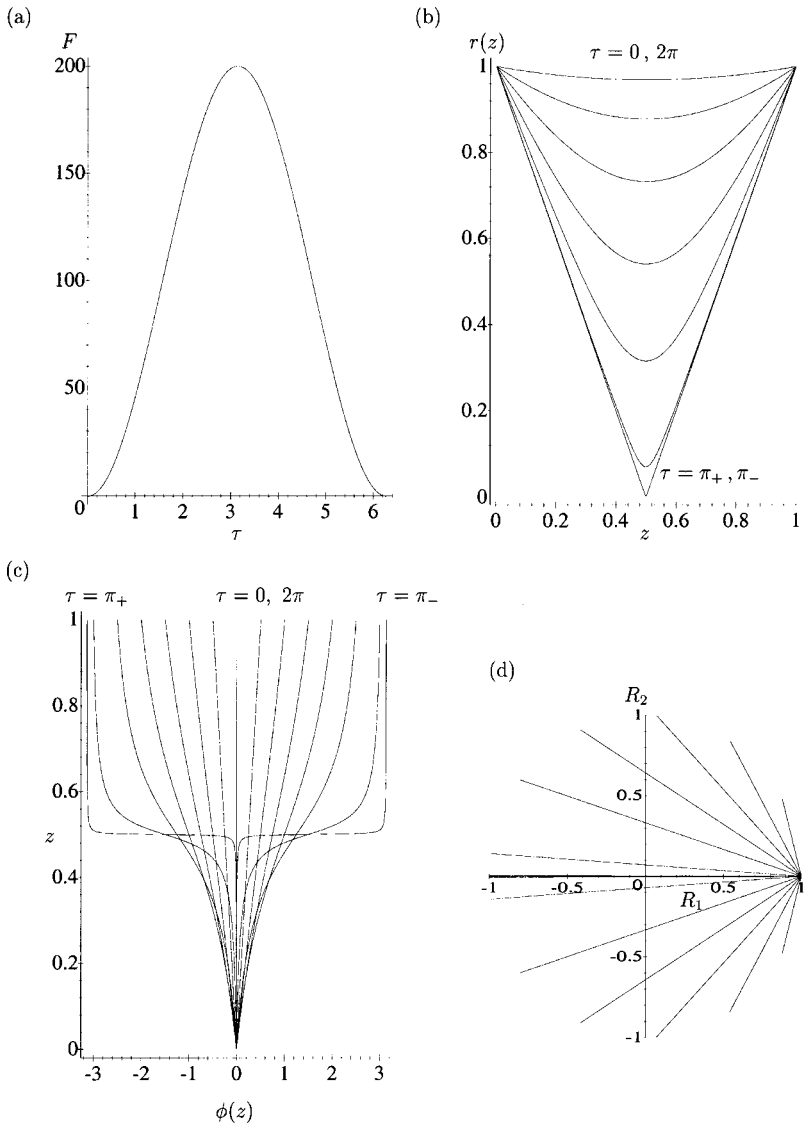

FIG. 4. Numerical solutions for $d=0.1$. (a) Energy F versus shear τ. (b) The density modulation amplitude $r(z)$. (c) The density modulation phase $\phi(z)$ (in radians). (d) The trajectories $\psi(z)$ in the complex plane.

$$r(1)=1, \quad \phi(1)=\tau. \tag{11b}$$

We may remark that this energy functional (10) resembles the Lagrangian functional for motion of a particle of mass $1/d^2$ in a frictionless bowl with potential minimum at radius $r=0$ and maximum around the rim at $r=1$. The particle moves from a starting point on the rim at $\phi=0$ and a finishing point again on the rim at $\phi=\tau$. There is in fact an isomorphism between the particle trajectories and the minimizers $\psi(z)$. High mass particles will tend to fall into the bowl easily, consistent with melting of the smectic in a thin cell ($d \gg 1$), whereas low mass particles will travel near the rim, consistent with layer tilt in a thick cell ($d \ll 1$). This analogy will be particularly apparent when we consider the trajectories of $\phi(z)$ in the complex plane.

The relevant Euler-Lagrange equations are now

$$r''+d^2 r(1-r^2)+r\phi'^2=0, \tag{12a}$$

$$(r^2\phi')'=0. \tag{12b}$$

In the dynamical analogy, these equations correspond respectively to conservation of energy and angular momentum, solutions of which may be expressed in terms of elliptic functions.

There are now two control parameters, namely the nondimensional thickness d and the shear τ. The significance of d can be examined in the free energy (10). When d is small, the $(1-r^2)^2$ term can be ignored and changes in the smectic amplitude r are not, relatively speaking, energetically expensive. Thus smectic melting can occur in the center of the sample. By contrast, for large d the reverse is true, r is constrained to be close to 1 and the system now prefers changes in ϕ, i.e., layer tilting.

We have so far emphasized the behavior of the smectic amplitude $r(z)$ and phase $\phi(z)$. However, we shall sometimes find it convenient to consider the real and imaginary parts of the smectic order parameter

$$\psi=R_1+iR_2. \tag{13}$$

This is particularly true at complete mismatch $\tau=\pm\pi$ when

d is small, for which, as we shall see explicitly in Sec. V, $\psi(z)=R_1(z)$ and melting of the smectic layers occurs at the center of the cell.

In the succeeding sections we investigate the behavior of the model described by the free energy (10) with associated boundary conditions. These studies are both numerical, using the continuation package AUTO97 [10,11], and, at critical points in the phase diagram, analytical.

IV. NUMERICAL STUDIES

Initially, the system is solved for all τ and for $d=0.1$ and $d=10.0$. From these solutions it is then possible to use AUTO97 to obtain the behavior for all values of d.

For all values of d the lowest energy solution is $r(z)=1$ and $\phi(z)=0$, which occurs at shear values of $\tau=0,2\pi,4\pi,\ldots$. Between these shear values the behavior is very different for different values of d. The solutions for $d=0.1$ and $d=10.0$ are shown in Fig. 4 and Fig. 5–7, respectively.

For $d=0.1$, Fig. 4 shows the free energy versus shear, the $r(z)$ and $\phi(z)$ solutions and the trajectories of ψ in the complex plane. Initially, as shear increases the phase is essentially linear across the cell while the order parameter r decreases in the center of the cell. For shear values approaching $\tau=\pi$, the phase change across the cell concentrates in the center. The associated large value of $d\phi/dz$ induces *melting* of the smectic layers characterized by the reduction of the order parameter $r(z)$ at this point. At $\tau=\pi$ the phase, ϕ and the derivative of $r(z)$ are discontinuous and $r(z=0.5)=0$. The energy is a maximum. For $\tau>\pi$ this process is essentially reversed as the system relaxes to the energy minimum at $\tau=2\pi$. As noted previously, the discontinuous jump in phase does not result in a discontinuous jump in the complex order parameter ψ. This can be seen in the trajectories in Fig. 4(d). The discontinuous jump in ϕ (and the gradient of r) at $\tau=\pi$ is not present in the R_1 and R_2 solutions.

For $d=10.0$ the behavior has changed significantly (Figs. 5–7). Figure 5 shows that for shear values $0.458<\tau<5.825$ there are three solutions, two stable and one unstable. The stable solutions occur along branches 1 and 2 while the unstable one occurs along branch 3. The stable branches are local minima of the free energy (7) while the unstable branch is a local maximum. At two *limit points* the unstable solution and one of the stable solutions meet and annihilate each other so that in the regions $0.0<\tau<0.458$ and $5.825<\tau<2\pi$ there exists only one solution.

As discussed in the previous section, at the point $\tau=\pi$ the two stable branches have the same energy whereas for $0.458<\tau<\pi$ branch 1 is the global minimum and for $\pi<\tau<5.825$ branch 2 is the global minimum. If the cell is sufficiently defect free it is therefore possible to *supershear* the layers as the system follows branch 1 past $\tau=\pi$. The system will stay in the local energy minimum on branch 1 even though it is at a higher energy than branch 2. Upon increasing τ further, branch 1 is annihilated by the unstable branch 3 and the system is forced to relax to a low *reverse* shear state on branch 2.

Figures 6 and 7 show the $r(z)$ and $\phi(z)$ solutions and the trajectories at various points on branches 1–3. In all these figures, solutions on branches 1 and 2 are characterized by almost linear shear across the cell with a small amount of melting in $r(z)$ while solutions on branch 3 are characterized by concentrated shear in the middle of the cell and a large amount of melting in $r(z)$.

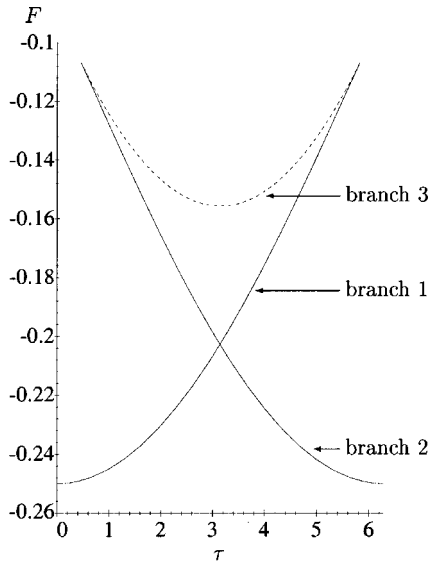

FIG. 5. Energy F versus shear τ for $d=10.0$. The solid lines denote the stable, solution branches 1 and 2 and the dashed line denotes the unstable, solution branch 3. For shear values between the limit points (where a stable branch meets the unstable branch) at $\tau=0.458$ and $\tau=5.825$ there exist three solutions, two stable and one unstable.

For shear values greater than $\tau=2\pi$, Fig. 5 is repeated periodically. Thus for a linearly sheared cell the shear stress would periodically increase and decrease as the system periodically followed branch 1 then fell to a relaxed state on branch 2.

We may examine the behavior of the system for values of d other than 0.1 and 10.0 by investigating how the two limit points vary as d is changed (Fig. 8). From Fig. 8(a) we see that as d decreases from 10.0 the two limit points converge and annihilate each other at the critical value $d=d_c=3.50$. For $d<d_c$, the behavior is essentially the same as that of $d=0.1$ described above. For $d>d_c$, the behavior is similar to that of $d=10.0$, however as d increases the two limit points diverge (linearly) and eventually move out of the region $0<\tau<2\pi$. Figure 9 shows such a situation for $d=12.0$. It is clear that in the region $5.732<\tau<6.834$ there are now three stable solution branches and two unstable solution branches since the branches from the adjoining region $(2\pi<\tau<4\pi)$ are now overlapping with the branches from the initial region $(0<\tau<2\pi)$. For large d, branches from other regions will overlap and there will exist more and more stable and unstable solutions. Figure 8(b) shows the crossing of the limit point loci. For all points in a diamond-shaped region the number of stable and unstable solutions is fixed. Figure 8(b) can therefore be thought of as a phase diagram. If the system crosses one of the limit point loci the number of possible solutions changes and a transition from one state to another (i.e., from the metastable stressed state mentioned above to a relaxed state) may occur. While there will be only one global energy minimizer at each point (τ,d) in Fig. 8(b)

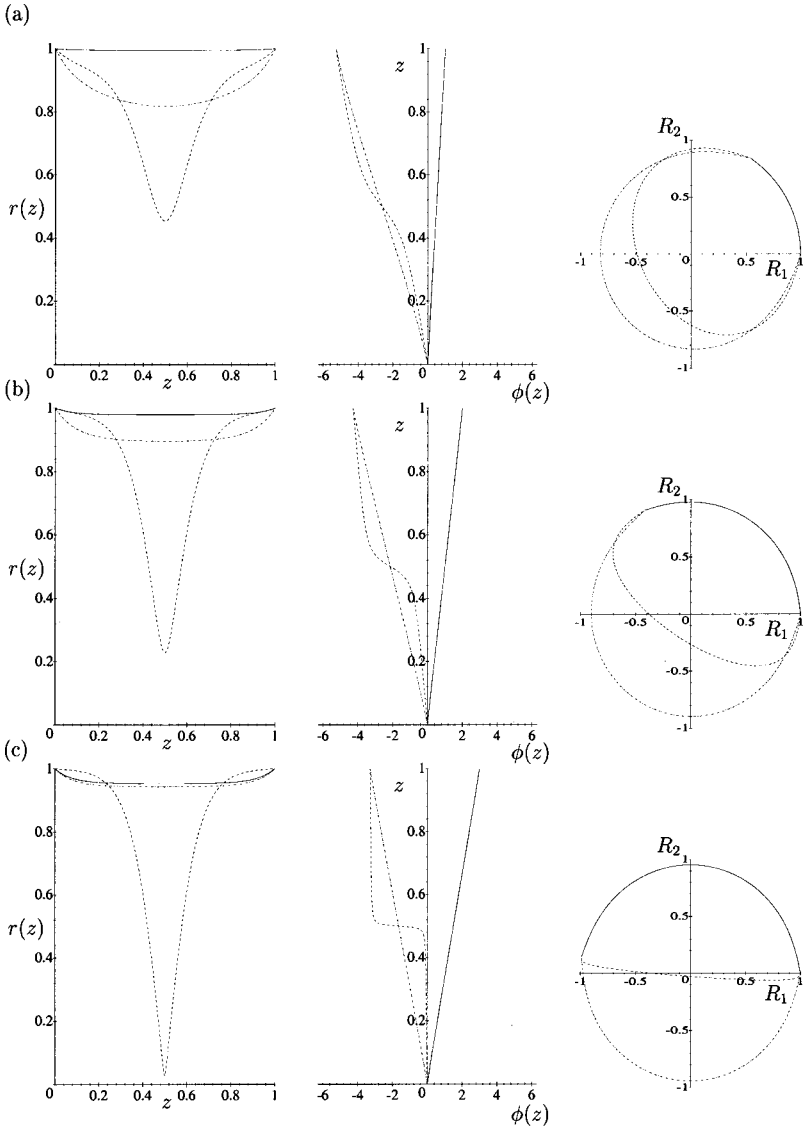

FIG. 6. $r(z)$ and $\phi(z)$ (in radians) solutions and the $\psi(z)$ trajectories for $d=10.0$ and shear values (a) $\tau=1$, (b) $\tau=2$, and (c) $\tau=3$. In each plot the solid, dashed-dotted and dashed line denote the stable solutions on branch 1 and 2 and the unstable solution on branch 3 (of Fig. 5), respectively.

there may be many metastable solutions that are locally stable.

Over much of the temperature range of the smectic-*A* phase, the smectic correlation length ξ is of the order of the size of a few molecules, typically 10 nm. An experimental cell dimension in the range 1–10 μm yields values for the nondimensional cell width $d\sim 100-1000$. This is large, and so we expect many metastable solutions.

For $d=100$, the energy vs shear plot is shown in Fig. 10, where only the stable solutions are shown for simplicity. At this parameter value, the limit point of branch 1 occurs at a shear of $\tau=56.69$, and for each shear value τ there are indeed many stable solutions.

Although characteristic values of d are large, we note that ξ is expected to increase dramatically close to a continuous nematic-smectic-*A* phase transition. In this region, d will thus decrease, and some of the interesting structure near to $d\approx d_c$ may be easier to observe.

V. ANALYTIC STUDIES

We are able to investigate certain regions of interest analytically. First, when the parameter d is small (as in Fig. 4), the system is relatively simple and the governing equations may be analytically solved. Second, from the numerical results we see that the region close to $\tau=\pi$ is very important and we are able to investigate this point in detail to determine the value of d for which the behavior changes from that similar to $d=0.1$ to that of $d=10.0$. Finally, the loci of the limit points may be investigated with the use of another approximate from of the governing equations.

A. The thin film limit

For very small values of d it is possible to simplify the system by considering only the highest order terms of the energy (7). Mathematically, this involves using d as a perturbation parameter and substituting the solution expansion

$$r(z)=r_0(z)+dr_1(z)+d^2r_2(z)+\cdots, \tag{14a}$$

$$\phi(z)=\phi_0(z)+d\phi_1(z)+d^2\phi_2(z)+\cdots \tag{14b}$$

into Eq. (12). The leading order equations are

$$0=\frac{d^2}{dz^2}r_0(z)-r_0(z)\left(\frac{d}{dz}\phi_0(z)\right)^2, \tag{15a}$$

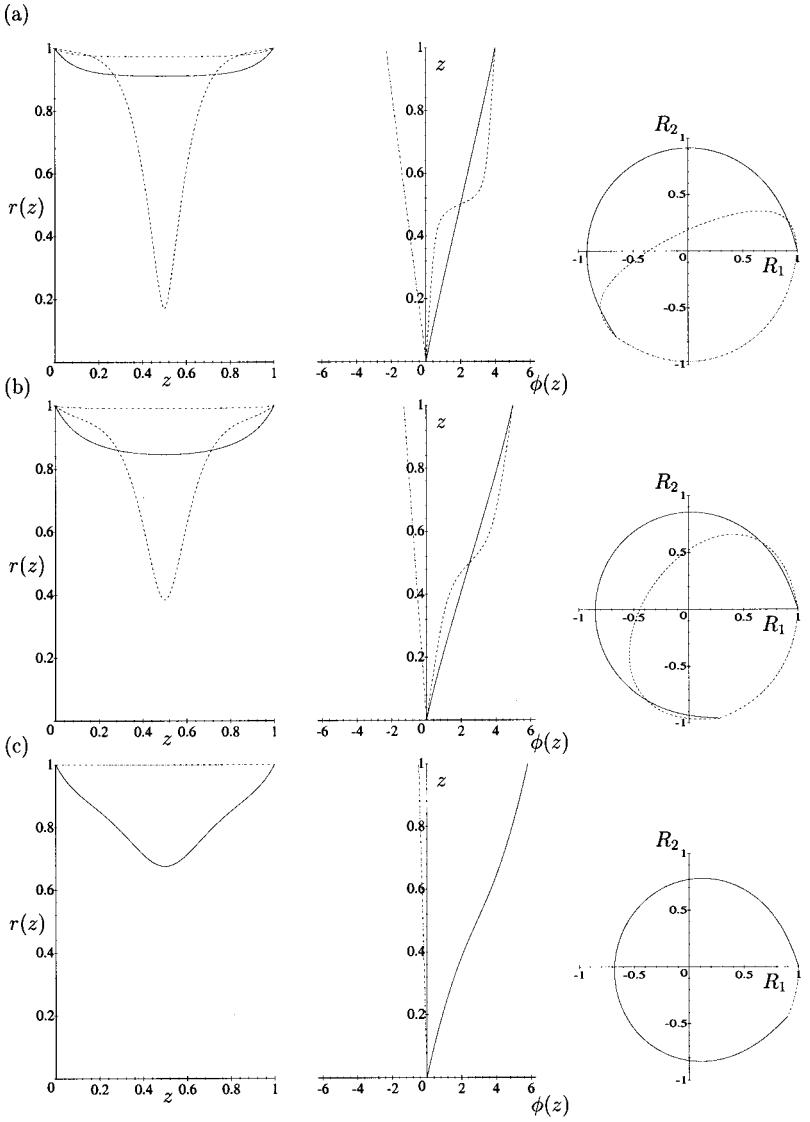

FIG. 7. $r(z)$ and $\phi(z)$ (in radians) solutions and the $\psi(z)$ trajectories for $d=10.0$ and shear values (a) $\tau=4$, (b) $\tau=5$, and (c) $\tau=5.825$ (the limit point). In each plot the solid, dashed-dotted and dashed line denote the stable solutions on branch 1 and 2 and the unstable solution on branch 3 (of Fig. 5), respectively. At the limit point the solutions from branches 1 and 3 coincide.

$$0=\frac{d}{dz}\left(r_0(z)^2\frac{d}{dz}\phi_0(z)\right). \tag{15b}$$

The solution to Eq. (15) subject to the boundary conditions (11) may be found by standard analytic techniques. The order parameter amplitude $r(z)$ is found to be

$$r_0(z)=\left[4z^2\sin^2\left(\frac{\tau}{2}\right)-4z\sin^2\left(\frac{\tau}{2}\right)+1\right]^{1/2}, \tag{16}$$

while the phase solution $\phi(z)$ is

$$\phi_0(z)=\frac{\tau}{2}-\arctan\left[(1-2z)\tan\left(\frac{\tau}{2}\right)\right]. \tag{17}$$

The corresponding highest order free-energy term is

$$F=\frac{2}{d^2}\sin^2\left(\frac{\tau}{2}\right). \tag{18}$$

Figure 11 shows the free energy vs shear, Eq. (18) for $d=0.1$, the $r(z)$ and $\phi(z)$ solutions, Eqs. (16) and (17), and the trajectories as τ varies. There is clearly very good agreement between this approximate analytic solution and the numerical solution for $d=0.1$ of the previous section (Fig. 4). In fact, we have found that the approximate solutions found above are still extremely close to the exact numerical solutions for values as large as $d=1$.

As we have seen in the last section, the condition $d\ll 1$ corresponds to $l\ll\xi$. Thus, except very close to the nematic-smectic-A phase transition, this corresponds to experimental cells of dimension $\sim$10 nm or less, which may not be reproducible experimentally.

B. Complete layer mismatch: the critical point

We have seen qualitatively in Sec. II that complete layer mismatch, when the layers on opposite faces of the cell are exactly misaligned and thus $\tau=\pi$, is of great qualitative importance in this system. This physical insight is echoed in the numerical studies in the last section. We now investigate the critical point at $\tau=\pi$, $d=d_c$ in more detail.

For thin films $d<d_c$ and the relevant solution at $\tau=\pi$ is a stable melted solution. By contrast, for $d>d_c$ this solution is unstable. The stability change is caused by the formation of two limit points at $d=d_c$. In order to analyze the loss of stability of the melted solution, it is useful to abandon the amplitude-phase variables and replace them by the real and

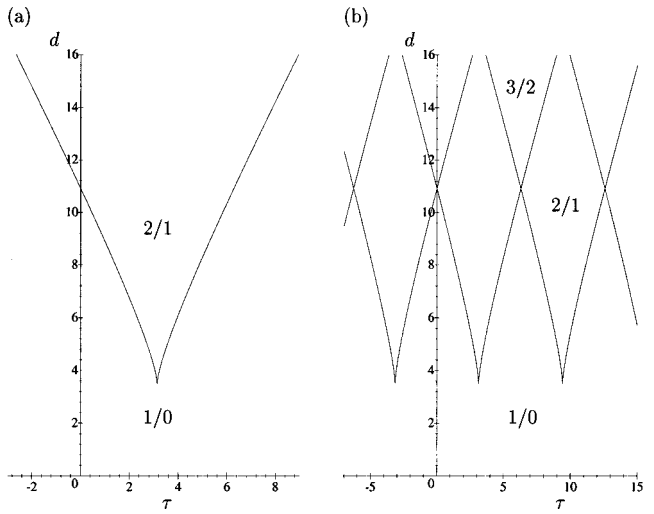

FIG. 8. The loci of the limit points in the τ-d plane. (a) The limit points formed at $d=3.50$, $\tau=\pi$ diverge as d increases. (b) The system symmetry implies that limit points are formed at the points $d=3.50$, $\tau=\pm\pi,\pm 3\pi,\pm 5\pi,\ldots$ and as d increases the limit points diverge and eventually *cross over*. The label i_s/i_u denotes the number of stable and unstable solutions (i_s and i_u, respectively) in each region.

imaginary parts R_1 and R_2 of ψ introduced in Eq. (13).

In these variables, the free energy (7) can be rewritten as

$$F=\int_0^1 dz\left[\frac{1}{4}([R_1^2+R_2^2]^2-1)^2+\frac{1}{2d^2}(R_1'^2+R_2'^2)\right]. \tag{19}$$

A good approximation to the melt solution at $\tau=\pi$ is $R_1=\cos(\pi z)$, $R_2=0$. To investigate its stability we will perturb this solution by a small amount, thus

$$R_1(z)=\cos(\pi z)+O(\eta^2), \tag{20a}$$

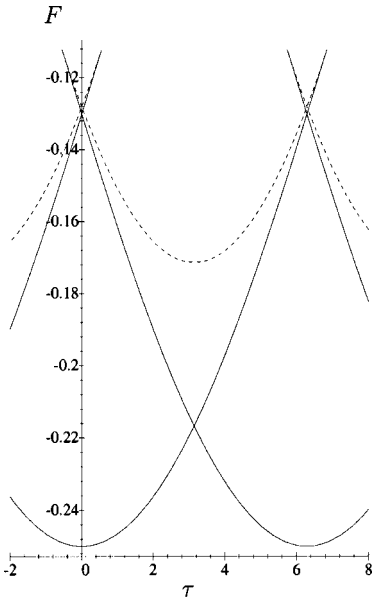

FIG. 9. Energy F versus shear τ for $d=12.0$. For shear values in the region $5.74<\tau<6.83$ there now exist five solutions, three stable and two unstable.

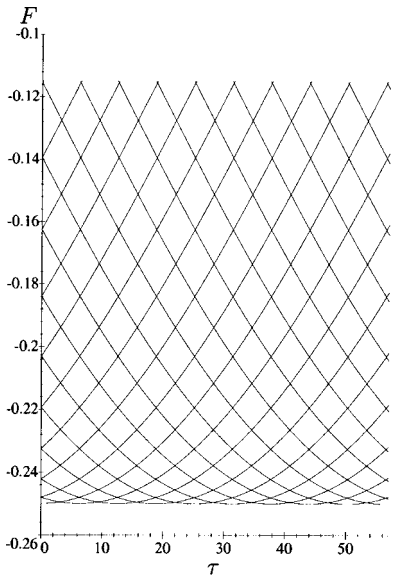

FIG. 10. Energy F versus shear τ for $d=100.0$, only the stable solutions are shown. There are now many stable solutions for each shear value.

$$R_2(z)=\eta\sin(\pi z)+O(\eta^3), \tag{20b}$$

where $\eta\ll 1$. The energy of the system can now be calculated in terms of the perturbation parameter η,

$$F(d,\tau=\pi,\eta)=F_0+\eta^2\left(\frac{\pi^2}{4d^2}-\frac{3}{16}\right)+\frac{3}{32}\eta^4, \tag{21}$$

where F_0 is the energy of the $\eta=0$ state.

This is a Landau expansion corresponding to a continuous transition from the $\eta=0$ state for $d<d_c$ to the $\eta\neq 0$ state for $d>d_c$, where

$$d_c=\frac{2\pi}{\sqrt{3}}\approx 3.63. \tag{22}$$

This value for the critical value of d is remarkably close to the numerical value of $d_c\approx 3.50$. Figure 12(a) shows $F(d,\tau=\pi,\eta)$ for various different values of d. For d close to d_c, the coefficient of η^2, which governs the stability of the $\eta=0$ state, may be approximated as $3/8(1-d/d_c)$, which is of the classic Landau form for such a transition.

For $d>d_c$, there are two equilibria, with positive and negative signs of η, which correspond to the solutions for $\tau=\pi$ on branches 1 and 2 in Fig. 5. These solutions break the symmetry of the free energy, in such a way that there is now a physical difference between a phase mismatch of $+\pi$ and $-\pi$. In Fig. 12(b), we show the phase trajectories of the solution for $d<d_c$ and $d>d_c$. For $d<d_c$, the phase trajectory goes through the origin, and thus the smectic layering melts at the center of the sample. Although there is a phase change of π on traversing the cell, the two states $\phi=0,\pi$ are in fact equivalent and the transition between them occurs at the point where $\rho=0$ and thus ϕ is not defined. By contrast, for $d>d_c$, there are two energetically equivalent trajectories, with opposite layer tilts. In the convention we adopt, $+\pi$ corresponds to layers that lean to the right, and $-\pi$ to layers that lean to the left.

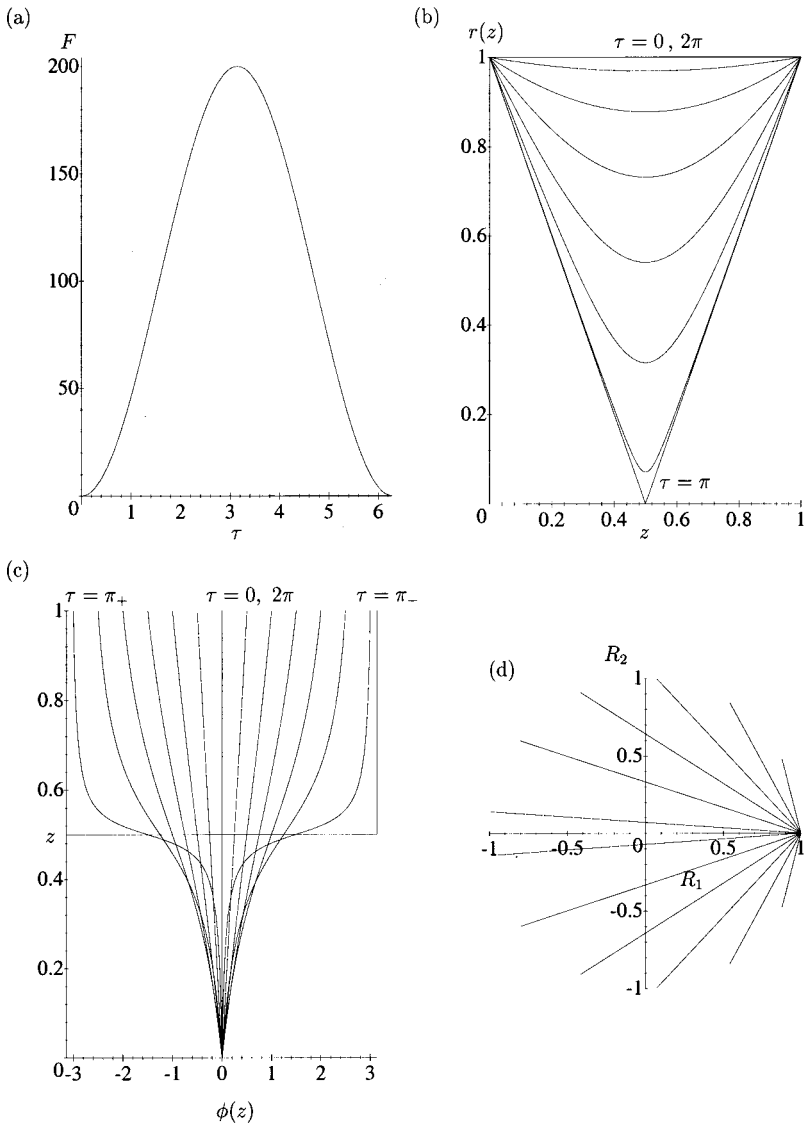

FIG. 11. Analytic solutions for $d \ll 1$. (a) The energy versus shear plot, (b) $r(z)$ and (c) $\phi(z)$ (in radians) solutions and (d) the $\psi(z)$ trajectories are in very good agreement with the numerically obtained solutions in Fig. 4.

It is, however, important to note that for $d \gg d_c$, a uniformly leaning layer would have the solution $\phi \approx \pi z$. By contrast, for $d \lesssim d_c$ the solution found above is $\phi \approx \tan^{-1}[\eta \tan(\pi z)]$, where $\eta \ll 1$ and the trajectories pass close to the origin [Fig. 12(b)]. The majority of the phase change then occurs at the center of the cell with the slope of the phase angle being approximately $\phi' = \pi/\eta$ [see Fig. 12(b)].

C. Complete layer mismatch: close to the critical point

We have seen in the last section that for $\tau = \pi$ and $d > d_c$, there are two energetically equivalent stable states corresponding to left-tilting and right-tilting layers and an unstable melted state. Thus if we examine $F(d > d_c, \tau = \pi + \delta)$, there will be an exchange of stability between the two stable states, or equivalently a first-order phase transition, as δ passes through zero.

This situation can be modeled using similar analysis to the last section. The free energy corresponding to Eq. (21) is equivalent to a Landau model of an Ising system in zero field with order parameter η. The inclusion of a small change in shear, δ, is then analogous to adding an external field term in which the field is proportional to δ. While the $-\eta$ solution is favored by δ positive, the $+\eta$ solution remains metastable. For sufficiently large δ it eventually loses stability at the critical value $\delta = \delta_c(d)$, beyond which layer slippage takes place. The equivalent occurs in the $+\eta$ case for δ negative.

Clearly as $d \to d_c$, $\delta_c \to 0$. Thus, as expected, the spinodal line approaches $\tau = \pi$ at $d = d_c$. What interests us here is the dependence of δ_c on d.

We use a modified form of the ansatz (20):

$$R_1(z) = \cos(\pi z), \tag{23a}$$

$$R_2(z) = \eta \sin(\pi z) - \frac{\delta}{2}. \tag{23b}$$

Note that we retain in this ansatz only terms to order δ. The phase mismatch here is $\pi + \delta$, but in order to simplify the mathematics, we have altered the boundary conditions so that $\phi(0) = -\delta/2$ and $\phi(1) = \delta/2 + \pi$. Since the physics is independent of the value of $\phi(0)$ and only depends on the mismatch this does not change the system.

The free energy (19) can now be computed, which to $O(\delta)$ is

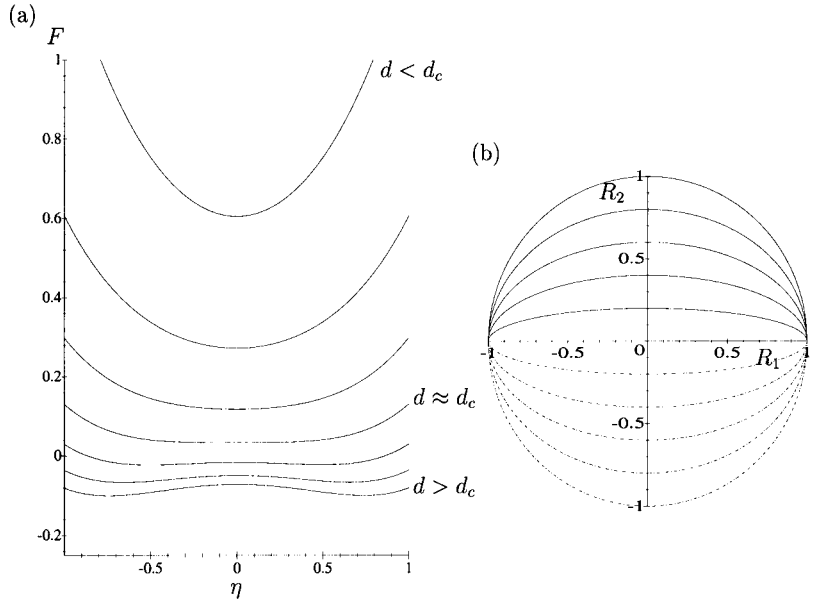

FIG. 12. (a) Energy at $\tau=\pi$ as a function of the perturbation parameter η as d varies. (b) $\psi(z)$ trajectories of the stable solutions. For $d<d_c$, the stable solution occurs for $\eta=0$ so that the trajectory lies along the R_1 axis between $R_1=0$ and $R_1=\pi$. For $d>d_c$, $\eta\neq 0$ and the two solutions lying in the energy minima correspond to trajectories passing through the point $R_1=0$, $R_2=\pm\eta$ in the complex plane. The positive and negative η solutions are represented by solid and dashed-dotted lines, respectively.

$$F(d,\delta,\eta)=F_0+\frac{3}{16}\left(\frac{d_c^2}{d^2}-1\right)\eta^2+\frac{3}{32}\eta^4+\frac{2}{3\pi}\delta\eta. \tag{24}$$

The spinodal line occurs for values of δ at which a maximum and a minimum coalesce. The condition for this is that

$$\frac{\partial F}{\partial \eta}=\frac{\partial^2 F}{\partial \eta^2}=0. \tag{25}$$

We thus obtain the following equations for $\delta_c(d)$:

$$0=\frac{2}{3\pi}\delta+\frac{3}{8}\eta^3+\frac{3}{8}\left(\frac{d_c^2}{d^2}-1\right)\eta, \tag{26a}$$

$$0=\frac{9}{8}\eta^2+\frac{3}{8}\left(\frac{d_c^2}{d^2}-1\right). \tag{26b}$$

Solving these equations yields the position of the critical spinodal line:

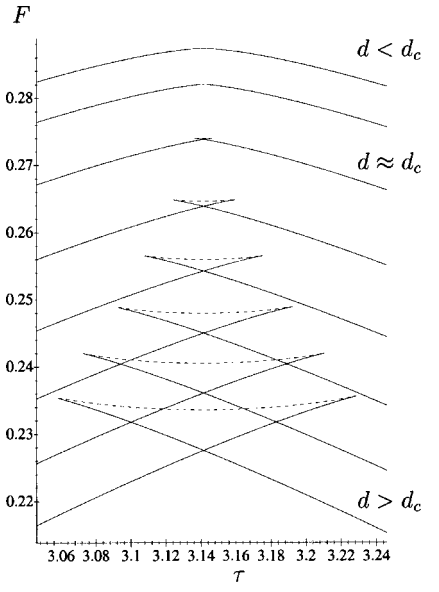

FIG. 13. Analytic solutions for the energy versus shear plots near to $\tau=\pi$ for various values of d. As in the numerical solutions for $d=d_c$, two limit points are formed at $\tau=\pi$ and diverge as d increases.

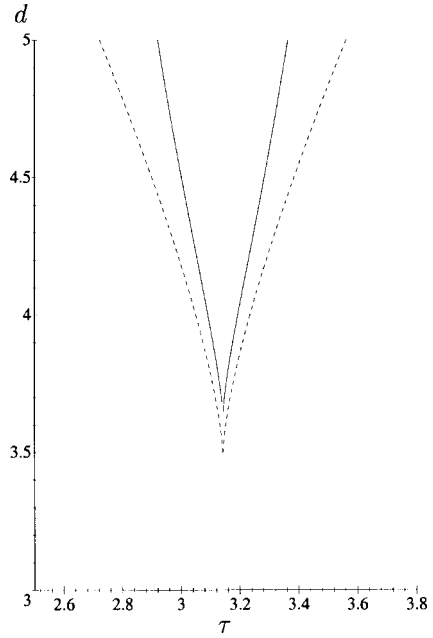

FIG. 14. The locus of the cusp points as d and τ vary. The solid and dashed lines line represent the analytic and numerical solutions, respectively.

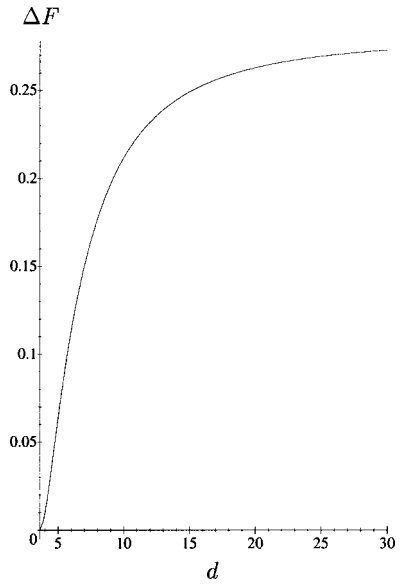

FIG. 15. The difference in energy between branch 1 and branch 2 (see Fig. 5) for the shear value at the limit point, ΔF, versus d.

$$\tau_c(d)=\pi\pm\delta_c(d)=\pi\pm\delta_0\left(\frac{d_c^2}{d^2}-1\right)^{3/2}, \tag{27}$$

with $\delta_0=\sqrt{3}\pi/8\approx 0.680$.

Figure 13 shows the energy versus τ plot for various values of d. We can clearly see how, as d passes d_c the stable solution at $\tau=\pi$ becomes unstable and two limit points form and then move apart. To compare this behavior to the numerical results, Fig. 14 shows the locus of the two cusps in the τ-d plane for both numerics and analysis. We find good agreement when $|\delta|\ll 1$, i.e., $\tau\approx\pi$ while the expansion (23) is valid. Thus this analysis is only valid for a limited range of d.

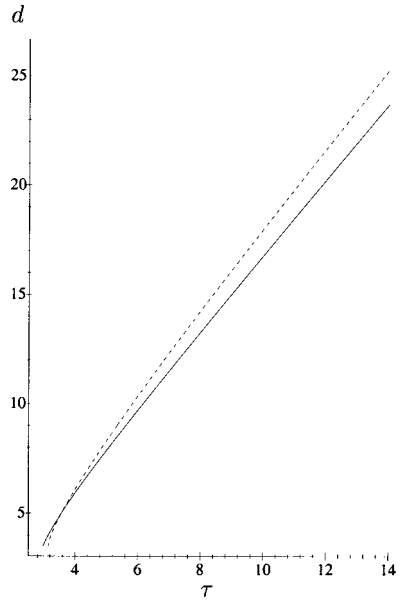

FIG. 16. The analytic locus of the limit point as d and τ vary found by following the approximate analytic solution at the limit point. The solid and dashed lines line represent the analytic and numerical solutions, respectively.

As shear increases and the system reaches the limit point (e.g., see Fig. 5) it will *fall* from the high energy state (on branch 1) to the relaxed low energy state (on branch 2). The change in energy as this metastable state disappears and the system relaxes can be calculated from the solutions of Eq. (26) with Eq. (27) substituted into the free energy Eq. (24). This difference in energy ΔF is (see Fig. 15)

$$\Delta F=\frac{9}{32}\left(1-\frac{d_c^2}{d^2}\right)^2=\frac{9}{32}\left(\frac{\delta}{\delta_0}\right)^{4/3}. \tag{28}$$

Therefore the energy jump from the metastable shear-stressed state to the relaxed state asymptotes to the value $\Delta F=9/32$ as seen in Fig. 15.

Although we have successfully investigated the behavior around $\tau=\pi$, finding analytic values for the critical parameter d_c, the location of the limit points and the difference in energy between the metastable stressed state and the relaxed state at the point where the former loses stability, we would like to be able to locate, analytically, the limit points for large values of d in order to model the more realistic values ($d\approx 100-1000$) mentioned in the previous section.

D. Limit point solution

In order to investigate the limit point further from $d\approx d_c$, we will use an approximate form of the solution at the limit point. This solution is of the form

$$r(z)=1-\epsilon\sin(\pi z), \tag{29}$$

with $\epsilon\ll 1$. We need not consider the $\phi(z)$ solution since manipulation of the second governing equation (12b) enables us to write the free energy (7) purely in terms of $r(z)$.

$$F=\int_0^1 dz\left[\frac{1}{2d^2}\left(\left(\frac{d}{dz}r(z)\right)^2+\frac{\tau^2}{4\int_0^1\frac{1}{r(z)^2}dz}\right)-\left(\frac{1}{2}r(z)^2-\frac{1}{4}r(z)^4\right)\right]. \tag{30}$$

When Eq. (29) is used, the free energy can be expanded in powers of ϵ

$$F=\frac{1}{4}\gamma^2-\frac{\gamma^2}{\pi}\epsilon+\left[\gamma^2\left(\frac{4}{\pi^2}-\frac{3}{8}\right)+\frac{\pi^2}{8d^2}+\frac{1}{4}\right]\epsilon^2+\left[\frac{\gamma^2}{\pi}\left(\frac{5}{3}-\frac{16}{\pi^2}\right)-\frac{2}{3\pi}\right]\epsilon^3+O(\epsilon^4), \tag{31}$$

where $\gamma=\tau/d$. The two solutions of $dF/d\epsilon=0$ correspond to the minimum and maximum of the free energy corresponding to branches 2 and 3 of Fig. 5. The limit point occurs when these two stationary points annihilate each other leaving a point of inflection. We therefore find the limit point by solving $dF/d\epsilon=0$ and $d^2F/d\epsilon^2=0$ simultaneously, for γ and ϵ. The solution, although analytically soluble, is lengthy except in the limit $d\to\infty$ when it reduces to

$$\gamma \to \gamma_c = \left(\frac{6\pi^4 - 16\pi^2\sqrt{32-2\pi^2}}{9\pi^4 + 128\pi^2 - 2048} \right)^{1/2} = 0.585. \quad (32)$$

The asymptotic value $1/\gamma_c = d/\tau_c$ is the analytic solution for the gradient of the limit point locus in Fig. 8(a). Figure 16 shows both the numerical and analytic locus of the cusp point as d and $\tau = \gamma d$ vary. The numerical asymptotic value of the gradient, 1.73, is in good agreement with the analytic value $1/\gamma_c = 1.71$.

The intersection points of the limit point loci in Fig. 8(b), where the number of stable and unstable solutions exist for specific shear values τ successively increases, can be calculated from the asymptotic value of γ. Since the limit point loci coincide when $\tau = 2\pi, 3\pi, 4\pi, \ldots$, the critical d values are

$$d_{c,n} = n\pi/\gamma, \quad (33)$$

where $n = 2,3,4 \ldots$. Using the numerically obtained value of γ_c, the first three critical points are $d_{c,1} = 10.87$, $d_{c,2} = 16.29$, and $d_{c,3} = 21.73$.

E. The dynamics of topological change

The theory that we present in this paper is quasistatic and cannot address the details of the dynamics of the breakdown of supershear. Nevertheless we shall find that our understanding of the quasistatic theory is able to give at least a qualitative picture of the dynamic process.

We begin this section by observing, from Eq. (31), that the limit point marking the collapse of supershear is a result of the mutual annihilation of a local free-energy minimum and the nearby maximum. Once τ reaches τ_c, the system relaxes to a new lower energy state. From a computational point of view, however, the problem is that this new free-energy minimum is no longer described by Eq. (31), for in the dynamic relaxation process the ansatz (29) fails. The new equilibrium structure $\psi(z)$ possesses an effective shear reduced by 2π, and thus the value of γ to be used in Eq. (31) is reduced by $2\pi/d$. A dynamical reformulation of the problem in terms of the order parameter components $R_1(z)$ and $R_2(z)$ avoids computational problems, but at the expense of the physical meaning provided by the shear τ.

We shall consider collapse of supershear in the large d limit in which case $\tau_c \gg \pi$.

For a specific shear value, τ the $\phi(z)$ trajectories in the complex plane are classified by their winding number or Morse Index j, which is the number of times the trajectory orbits the origin and is related to the effective shear of the solution. A trajectory with winding number j corresponds to layers tilting by a distance x_{displ}, where $ja < x_{\mathrm{displ}} < (j+1)a$ through the cell.

Let us summarize the important features of these trajectories. As they loop around the origin, they spiral inward over an angle $j\pi$, and then outward, in a symmetrical way. For large j, the trajectory approaches the origin more closely so that the innermost loop is the smallest.

Qualitatively we can now see what will occur as the limit point is reached. The trajectory with winding number j will become unstable and relax to that with winding number $(j-1)$. This involves the innermost loop of the trajectory collapsing, and the other loops readjusting themselves. The important steps in this dynamic process are illustrated in Fig. 17 where we have concentrated on the innermost loop of the trajectory.

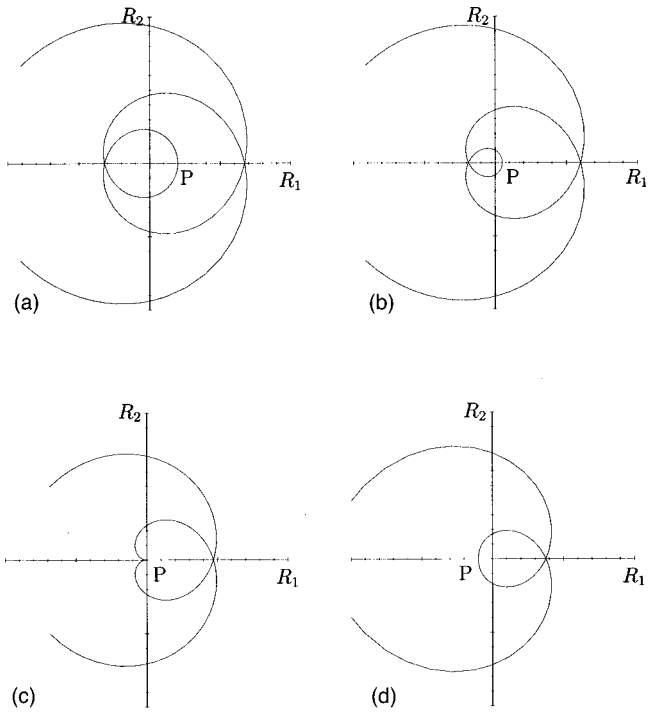

FIG. 17. The dynamic process as the system relaxes from the supersheared state at the limit point. (a) The innermost loop of the original trajectory encircling the origin of the complex plane with winding number j. (b) The loop starts to collapse. (c) The trajectory passes through the origin as the loop disappears at a cusp. (d) The new stable orbit now has winding number $(j-1)$.

As the system *falls* from the limit point, the innermost loop of the original trajectory encircling the origin of the complex plane [Fig. 17(a)] starts to collapse [Fig. 17(b)] and in particular the position closest to the origin, P, approaches the origin. In Fig. 17(c) the trajectory actually passes through the origin as the loop disappears at a cusp and in Fig. 17(d) the orbit now has winding number $(j-1)$. The original trajectory with winding number j has now decayed to a new stable trajectory with winding number $(j-1)$.

Figure 18 shows this process in terms of the layer configurations. By symmetry, P corresponds to the exact center of the cell $z = \frac{1}{2}$. As P approaches the origin, the layer tilt at the center of the cell increases [Fig. 18(b)], until the layers are parallel to the cell when P coincides with the origin [Fig. 18(c)]. However, since the trajectory goes through the origin, the order parameter at $z = \frac{1}{2}$ is zero, and the phase is undefined. In fact, as can be seen by examining Fig. 18(c), there is a discontinuity in phase across $z = \frac{1}{2}$ of exactly π. Just *before* the orbit goes through the origin, the phase change close to the center of the cell is 2π. But just *after* the orbit has gone through the origin, the phase jump is zero. As P passes through the origin, the layers have separated and reattached, in the process losing a phase change of 2π.

The details of this description will depend on the dynamical structure of the equations governing smectic-A layer motion. A simple time-dependent version of equations that allows only for dissipative behavior is the Ginzburg-Landau

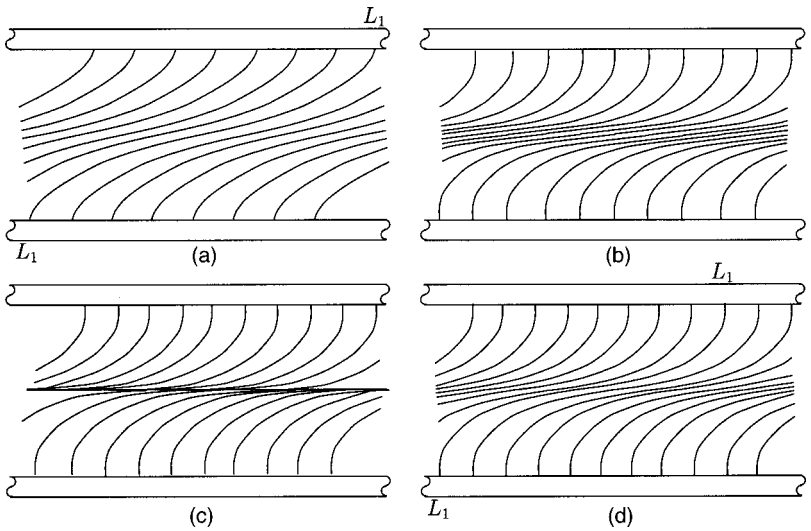

FIG. 18. The dynamic process in Fig. 17 in terms of the layer configurations. (a) The supersheared layer configuration. (b) The layer tilt at the center of the cell increases until the layers are parallel to the cell at the center where melting occurs, (c). (d) The layers reform in a relaxed state such that the layer denoted by L_1 in (a) now has a phase change between the cell surfaces reduced by 2π.

equation. The dynamics of the 2π reduction in phase seen above has previously been studied in detail [12–15]. However, the full equations are inevitably more complicated and include smectic-*A* hydrodynamics in the presence of layer conservation. Whatever these details, they will not alter the stable qualitative dynamical features discussed here.

VI. DISCUSSION

In this paper, we have presented a detailed analysis of shear-induced melting in smectic-*A* liquid crystals. The calculations reveal a complex phase diagram described by the two system control parameters, the nondimensionalized gap width d and the imposed shear τ.

We have found that there is a critical value of the thickness d_c at which the cell behavior changes qualitatively. For $d \leqslant d_c$, the layers continuously melt and reform as the shear increases through $n\pi$ for odd n. In this way, the effective layer tilt is always $|\tau| < \pi$ and when the layers melt they do so when the smectic order parameter at the center of the cell is zero. The free-energy minima occur when there is a possibility of layer matching in a perfect bookshelf structure, which occurs for $\tau = 2n\pi$. The maxima occur for $\tau = (2n+1)\pi$, when the phase is discontinuous at the center of the cell and the layers on each side of the cell are exactly out of phase.

For $d > d_c$, however, the behavior is significantly different. It is now possible to supershear the layers into a metastable state with $|\tau| > \pi$ until a critical value of the shear $\tau_c(d)$. For $d \to d_c^+$, $\tau_c(d) \to \pi$, and with increasing thickness, the critical shear value is linear with respect to d [i.e., $\tau_c(d) \to \gamma_c d$]. For large values of d, there will, in general, be a large number of metastable states, each associated with a different winding number corresponding to the number of layers crossed as one traverses the cell normal to its surfaces. When the system reaches the critical shear value, the system relaxes into the next highest free-energy metastable state reducing the winding number by one and melting at the center of the cell as it relaxes.

Whether experiments actually exhibit this behavior depends on a number of factors. First, we note our assumption of homogeneity through the plane of the cell. The existence of many metastable states implies the possibility of transformation through a dislocation rather than by homogeneous nucleation. In this case a new state with lower winding number is formed as a front, containing a dislocation line, moves within the cell. This dislocation would then possess a Burgers vector that compensates for the extra winding number.

Second, we have assumed that the cell surface imposes strong anchoring such that the layer positions are fixed at the boundaries. As we observed in the Introduction, this assumption derives from the existence of the chevron structure that is usually justified in terms of a surface memory effect. In practice there is no microscopic description of this process, and detailed experimental evidence and description of the phenomenon is lacking. Introducing weaker surface anchoring allows layer sliding to take place at the surface as well as at the center of the cell.

The experiments of Cagnon and Durand [3] showed that the response supersheared to a sheared smectic *A* in the bookshelf geometry had two components. The major component was a linear behavior superposed on which was a smaller periodic response. Linear behavior is just what is expected for $\tau < \tau_c$; the stored free energy is proportional to τ^2 just as in Hooke's law, as can be seen in Figs. 9 and 10. In contrast, periodic behavior is what is expected for $\tau \sim \tau_c$, for now the system is reaching its critical value, relaxing, increasing to its critical value, relaxing and so on. The temptation is to suppose that the existence of defects divides the system into parts where (locally) $\tau < \tau_c$, and other parts where $\tau \sim \tau_c$. A superposition of these two qualitatively different behaviors could describe the results of Cagnon and Durand. Whether this really is the case is an open question, requiring both more experimental and theoretical investigation.

Finally, we observe that the root of the phenomenon we are investigating is a periodic response to a linear force, and the fundamental reason for this is that the underlying dynamical variable in the problem is a *phase*. The periodic

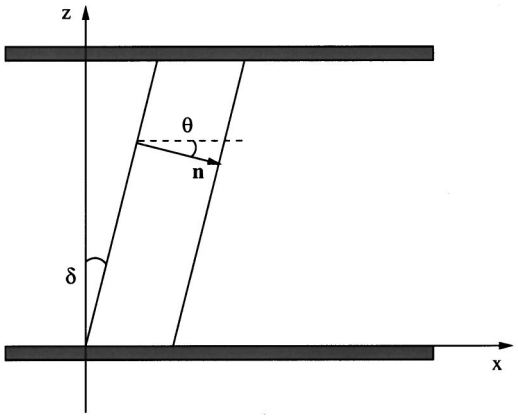

FIG. 19. Configuration of the tilted layer with layer tilt δ and director angle θ.

process involves changes in a topological variable with some defect motion. In this sense the smectic A has many topological analogies. One such analogy is the classical Josephson effect [16,17] in which an *alternating* current can be produced by a *constant* voltage difference across a weak superconducting link. The current is associated with the motion of magnetic flux quanta across the weak link. The flux quanta are defects in the superconducting order parameter, which, like the smectic-A order parameter, is a two-component or XY-like spin field.

ACKNOWLEDGMENTS

T.J.S. would like to thank G. Durand for a number of useful conversations. N.J.M. would like to acknowledge the financial support of Sharp Laboratories of Europe Ltd. and the EPSRC.

APPENDIX: THE $\theta=0$ APPROXIMATION

We start with the free-energy equation (2),

$$F=\int d\mathbf{r}\Big\{ a|\Psi|^2+\frac{b}{2}|\Psi|^4+\zeta_{\|}|(\hat{\mathbf{n}}\cdot\boldsymbol{\nabla}-iq)\Psi|^2 + \zeta_{\perp}|(\hat{\mathbf{n}}\times\boldsymbol{\nabla})\Psi|^2+\tfrac{1}{2}K_{11}(\boldsymbol{\nabla}\cdot\hat{\mathbf{n}})^2+\tfrac{1}{2}K_{33}[\hat{\mathbf{n}}\times(\boldsymbol{\nabla}\times\hat{\mathbf{n}})]^2\Big\}. \tag{A1}$$

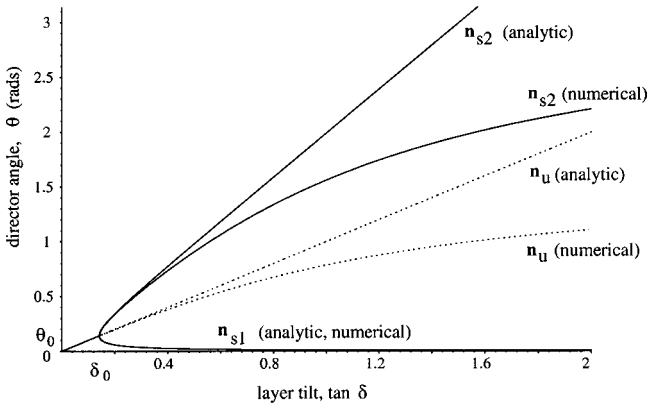

FIG. 20. Numerical and analytic solutions of the director tilt as a function of layer tilt, $\theta(\delta)$. Solid and dashed lines indicate stable and unstable solutions, respectively.

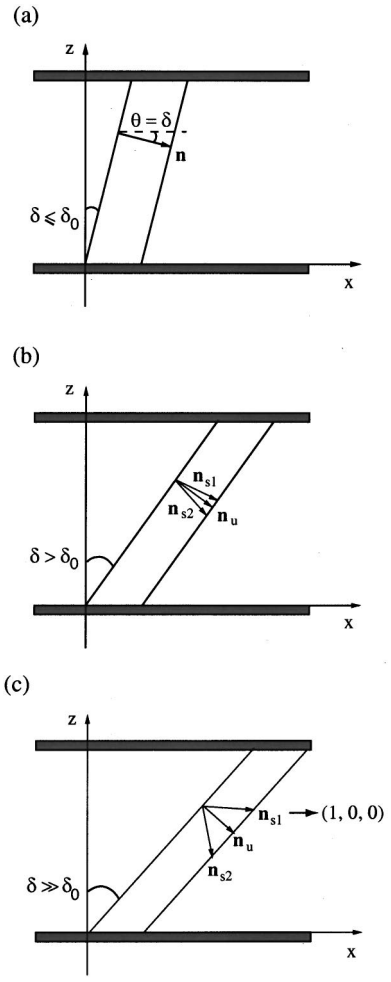

FIG. 21. (a) For $\delta \ll \delta_0$, there exists one solution $\theta \approx \delta$. (b) For $\delta > \delta_0$, there exist three solutions, one unstable $\mathbf{n}_u$ for which $\theta \approx \delta$, and two stable solutions $\mathbf{n}_{s1}$ and $\mathbf{n}_{s2}$, for which $\theta < \delta$ and $\theta > \delta$, respectively. (c) For $\delta \gg \delta_0$, the stable solution $\mathbf{n}_{s1}$ asymptotes to (1,0,0), i.e., $\theta \to 0$.

Let us consider the case when the order parameter amplitude ρ remains close to its equilibrium value $\rho_c = (-a/b)^{1/2}$ and thus we are able to assume $d\rho/dz \approx 0$ and disregard any derivatives of ρ. Using the nematic director $\mathbf{n} = (\cos\theta, 0, -\sin\theta)$, the smectic order parameter $\Psi = \rho_c e^{i(qx+\phi(z))}$, and relating the phase gradient with the layer tilt angle thus $d\phi/dz = -q\,du/dz = -q\tan\delta$, where u is the layer displacement and δ is the layer tilt angle (see Fig. 19), the free energy becomes

$$F=\int dr\Big\{ \zeta_{\|}q^2\rho_c^2(\sin\theta\tan\delta+(\cos\theta-1))^2 + \zeta_{\perp}q^2\rho_c^2(\sin\theta-\cos\theta\tan\delta)^2 + \frac{1}{2}\left(\frac{d\theta}{dz}\right)^2(K_{11}\cos^2\theta+K_{33}\sin^2\theta)\Big\}. \tag{A2}$$

By minimizing the first two terms, to find the bulk behavior of the response of the director tilt to tilting of the layers, we obtain the equation

$$0=\left(1-\frac{\zeta_\perp}{\zeta_\parallel}\right)[(\tan^2\delta-1)\sin(2\theta)+2\tan\delta\cos(2\theta)] +2\sin\theta-2\tan\delta\cos\theta, \tag{A3}$$

which gives the the director angle θ as a function of the layer tilt and the parameter $\zeta_\perp/\zeta_\parallel$.

Figure 20 shows the numerical solutions of Eq. (A3) that initiate from the bookshelf state ($\delta=0$, $\theta=0$). From Fig. 20, for which we have taken the parameter value $\zeta_\perp/\zeta_\parallel=10^{-2}$, we see that the initial behavior is $\theta\approx\tan\delta$ (or alternatively $\theta\approx q^{-1}d\phi/dz$).

However, for a finite value of $\zeta_\perp/\zeta_\parallel$ there exists a bifurcation of this solution at a critical value of layer tilt δ_0. The solution, $\theta\approx\tan\delta$, becomes unstable ($\mathbf{n}_u$ in Fig. 20) and two stable solutions are formed. For one of these stable solutions θ continues to increase ($\mathbf{n}_{s2}$ in Fig. 20) while for the other stable solution θ decreases asymptotically to zero ($\mathbf{n}_{s1}$ in Fig. 20). An illustration of this behavior is given in Fig. 21. The physical interpretation of these two branches is that the director is now tilting with respect to the layer normal in order to better satisfy the compressibility condition. (There is in fact a whole cone of such solutions just as in the smectic-*C* phase that correspond to molecules tilting in order to fit into the compressed layers.)

It is now necessary to reintroduce the elastic term from the free energy (A2) in order to determine which of the two stable in-plane solutions is selected by the system at the critical point $\delta=\delta_0$. It is obvious from the form of the elastic free energy [$\approx(d\theta/dz)^2$] that large distortions of θ are disfavored. Since we have fixed $\theta=0$ on the boundaries, the solution corresponding to $\theta>\delta$ is of higher energy than the solution where $\theta<\delta$ (in fact the in-plane solution with $\theta<\delta$ will also be the minimum energy configuration with respect to all out-of-plane tilted solutions). Thus the system selects the $\mathbf{n}_{s1}$ solution for $\delta>\delta_0$. The director angle now decreases and asymptotes to $\theta=0$.

Now, in order to investigate this behavior analytically, let us suppose that $\zeta_\perp/\zeta_\parallel=\epsilon\ll1$ and $\theta\ll1$, $\delta\ll1$. This last condition on δ is actually not necessary in order to find analytic solutions. However, without the $\delta\ll1$ condition, a cubic polynomial must be solved rather than a quadratic and since the behavior with or without this approximation is almost identical, we prefer the simpler solution expressions below. In this limit the first two terms of the free energy (A2) become

$$\zeta_\parallel q^2\rho_c^2\left[\left(\theta\delta-\frac{\theta^2}{2}\right)^2+\epsilon(\theta-\delta)^2\right]\sim\theta^2\left(\delta-\frac{\theta}{2}\right)^2+\epsilon(\theta-\delta)^2. \tag{A4}$$

Note the physical interpretation of these terms: The first is the compressibility term with minima at $\theta=0,2\delta$ and a maximum at $\theta=\delta$ whereas the second is the tilt energy term that has a minimum at the smectic-*A* state, $\theta=\delta$. Minimizing these terms, we obtain the solutions

$$\theta=\delta, \tag{A5}$$

$$\theta=\delta-\sqrt{\delta^2-2\epsilon}, \tag{A6}$$

$$\theta=\delta+\sqrt{\delta^2-2\epsilon}. \tag{A7}$$

These solutions are shown in Fig. 20 and marked with $\mathbf{n}_u$, $\mathbf{n}_{s1}$, and $\mathbf{n}_{s2}$, respectively. For $\delta<\sqrt{2\epsilon}$ the solution is $\theta=\delta$. This solution becomes unstable at $\delta=\sqrt{2\epsilon}$ when two stable solutions are formed [solutions (A6) and (A7) above]. We see good agreement between solution (A6) and the exact numerical solution since θ remains small for this solution.

From this analytic result we see that as δ grows large the director angle asymptotes to zero and in this limit $\theta\to\epsilon/\delta$. In this regime the free energy (A4) becomes

$$\zeta_\parallel q^2\rho_c^2\left[\epsilon^2+(\epsilon\delta^2-2\epsilon^2)+O\left(\left(\frac{\epsilon}{\delta}\right)^4\right)\right]. \tag{A8}$$

The second and third terms are the tilt energy terms while the first term is the compressibility term that is both smaller than the leading order tilt energy term and *constant*.

While it is clear that our assumption, that the free energy may be written as

$$F=\int_0^l dz\left[a\rho^2+\frac{b}{2}\rho^4+\zeta_\perp\left\{\left(\frac{d\rho}{dz}\right)^2+\rho^2\left(\frac{d\phi}{dz}\right)^2\right\}\right], \tag{A9}$$

is not valid for small amounts of layer tilt ($|d\phi/dz|\leqslant q\sqrt{2\zeta_\perp/\zeta_\parallel}$), it is however valid for larger layer tilts. It is in this regime where the important aspects of our work occur, i.e., where there exists a region of supershear and a spinodal point at a critical shear value.

One other possible limitation on the validity of the free-energy expression occurs at large shear values. In such instances the phase gradient may become large, thus invalidating a Landau-like expansion of the free energy. However, if we assume that the system is sufficiently close to the nematic-smectic-*A* phase transition (where $\rho\sim0$) the phase gradient terms in the free energy [$\rho^2\,d\phi/dz,\rho^2(d\phi/dz)^2$] remain small and the free-energy expansion is valid.

[1] P. G. de Gennes and J. Prost, *The Physics of Liquid Crystals* (OUP, Oxford, 1993).

[2] N. A. Clark and T. P. Rieker, Phys. Rev. A **37**, 1053 (1988).

[3] M. Cagnon and G. Durand, Phys. Rev. Lett. **70**, 2742 (1993).

[4] S. J. Elston and M. J. Towler, Phys. Rev. E **57**, 6706 (1998).

[5] P. G. de Gennes, Solid State Commun. **10**, 753 (1972).

[6] B. Andereck and B. Patton, J. Phys. (Paris) **48**, 1214 (1988).

[7] B. Patton and B. Andereck, Phys. Rev. Lett. **69**, 1556 (1992).

[8] B. Andereck, Int. J. Mod. Phys. B **9**, 2139 (1995).
[9] S. Kralj and T. Sluckin, Phys. Rev. E **48**, 3244 (1993).
[10] E. J. Doedel, Congressus Numeranti **30**, 265 (1981).
[11] E. J. Doedel and X. J. Wang, Center for Research on Parallel Computing, California Institute of Technology Report No.CRPC-95-2 (unpublished).
[12] P. H. M. C. Cross, P. G. Daniels, and E. Siggia, J. Fluid Mech. **127**, 155 (1983).
[13] L. Kramer and W. Zimmerman, Physica D **16**, 221 (1985).
[14] H.-G. P. H. Riecke, Phys. Rev. A **33**, 547 (1986).
[15] L. S. Tuckerman and D. Barkley, Physica D **46**, 57 (1990).
[16] B. Josephson, Adv. Phys. **14**, 419 (1965).
[17] J. Langer and V. Ambegaokar, Phys. Rev. **164**, 498 (1967).